11 Testing techniques

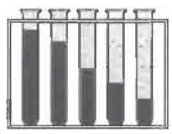

11.1 Rock properties

The term 'rock properties' refers here to those intact rock or rock mass properties that are needed for engineering design purposes. For example, the rock properties may be used to

- obtain a general impression of the mechanical nature of the rock mass, e.g. the rock is strong because it has a compressive strength of 300 MPa,
- compare the rock properties with a previous project where the rock properties were also obtained, e.g. this rock is stronger than the one we had at the Golconda Mine,
- generate a rock mass classification scheme value, e.g. the RQD is needed for the Rock Mass Rating (RMR) scheme, see Chapter 12, or
- support numerical modelling, e.g. the shear stiffness of fractures is required for a distinct element numerical code.

Many of the required rock properties can be categorized according to the subjects of the earlier chapters, as shown in Table 11.1.

Strictly speaking, *in situ* stress is a site property rather than a rock property, but testing techniques are required to determine the *in situ* stress and so it is one of the categories below. The 'permeability' could be included as a separate item under each of the 'intact rock', 'fractures' and 'rock mass', but we prefer to consider the property in a separate category because the subject involves the connectivity of the rock mass fractures. In each case, there should be information about any variation in these properties across the site, which was the theme of Chapter 10.

Table 11.1 Examples of rock properties measured in a site investigation programme

In situ stress	Intact rock	Fractures	Rock mass	Permeability
Magnitudes and directions of the three principal stresses	Deformation, strength and failure properties	Geometrical occurrence and mechanical properties	Deformation, strength and failure properties	Nature of any flow through the intact rock and rock mass

The structural geology and hydrogeological setting information will be strategically helpful for this purpose.

The rock properties can be measured directly or indirectly. For example, in Q10.3, the uniaxial compression test and point load test values were compared. Because the uniaxial compression test provides a direct value for the compressive strength, it is a direct test. On the other hand, because the point load test gives an index value which is used to indicate the uniaxial compressive strength via a correlation factor, the point load test is an index test. There are many possibilities for such indirect tests in rock mechanics and an advantage of them is that they can provide many more results than direct tests, more rapidly and more cheaply. Their disadvantage is a possible lack of precision and knowing whether or not there is any bias in the values. To make decisions about which type of test to use, one has to recall why the rock properties are required and the resources available, and hence whether direct tests, indirect tests, or a mix of the two types are best suited to the project in hand.

In the questions that follow in Section 11.2, we provide a flavour of the nature of site investigation and how some of the testing problems are solved. This chapter is the first where we link the rock mechanics with the rock engineering. It is important when practising rock engineering to understand the rock mechanics concepts first — which has been our aim in Chapters 1–10. Now, we highlight the engineering thinking that is required to assess and measure the rock properties.

11.2 Questions and answers: testing techniques

Q11.1 **The section of site investigation borehole core shown in the photograph on the next page is from a vertical borehole and contains three stress-induced fractures. The top of the core is a stress fracture of the same kind. The bottom end is a drilling break. Assuming that the strip of translucent tape (adjacent to the numbers written on the core in the photograph) is on the northern side of the core, in which horizontal directions do you think the major and minor principal stresses act?**

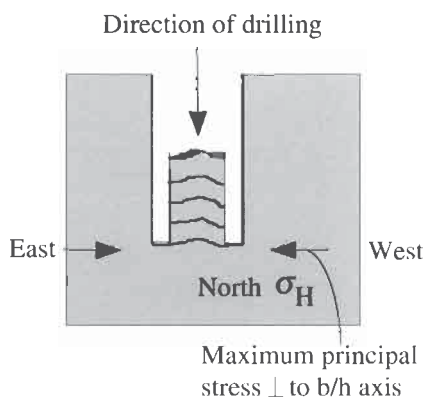

A11.1 The three central fractures and the top end of the core section are all fractures caused by the *in situ* stresses being concentrated at the end of the borehole during core drilling with a hollow drill bit, see diagram to right (Haimson, 1997[1];

[1] Haimson B. (1997) Borehole Breakouts and Core Disking as Tools for Estimating *In Situ* Stress in Deep Holes, in *Proc. of the Rock Stress Conference* (K. Sugawara and Obara Y., eds). Balkema, Rotterdam, pp. 35–42.

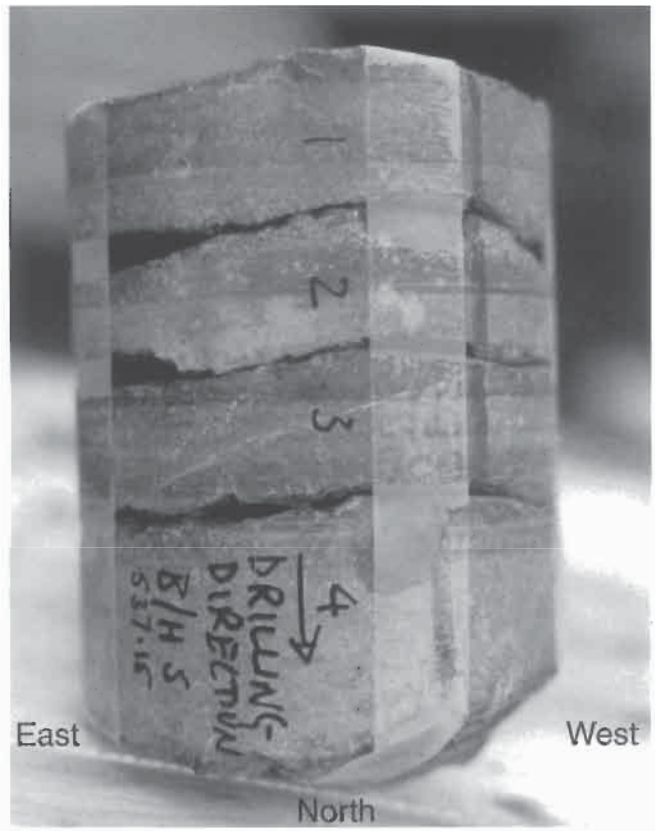

Bankwitz and Bankwitz, 1995[2]). The direction of the trough in the disc indicates the E–W direction of the σ_H major horizontal principal stress because the discs form in a similar way to the Brazilian tensile test failure — initiating on the diameter corresponding to the primary loading direction and propagating perpendicular to the least stress (which is vertical). The saddle shape occurs because the failure propagation follows the

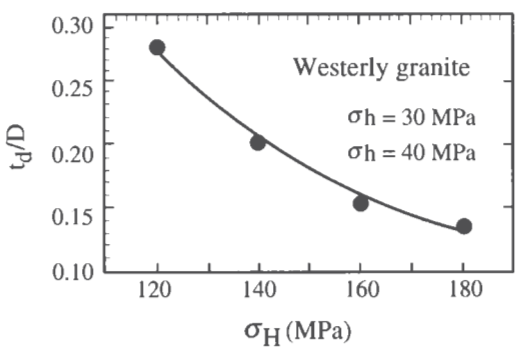

Example of the relation between core disk thickness (normalized by the core diameter) and σ_H for given σ_h and σ_v, from Haimson, 1997.

[2] Bankwitz P. and Bankwitz E. (1995) Fractographic Features on Joints of KTB Drill Cores (Bavaria, Germany), in *Fractography, Fracture Topography as a Tool in Fracture Mechanics and Stress Analysis* (M. S. Ameen, ed.). Geological Society Special Publication No. 92, pp. 39–58.

line of least resistance, rising towards the lower stressed region in the drill core. Thus, the major principal stress, σ_H, acts E–W and the minor principal stress, σ_h, acts N–S. The ratio of disc thickness to diameter indicates (according to the diagram included above from Haimson, 1997) that the local σ_H could be about 120 MPa.

***Q11.2* With reference to fracture property measurements made during a site investigation**
– on borehole rock core,
– on the borehole walls, and
– on rock exposures.
Complete the table below indicating your opinion of how well you think that the listed fracture properties can be measured or estimated. The first column of the table represents the ten fracture measurements recommended by the ISRM, as in Fig. 7.7. Use the letters G for Good, M for Medium, and P for Poor.

Characteristic	Measurement method	Core	B/H wall	Exposure
Orientation	Compass-clinometer			
Spacing	Measuring tape			
Persistence	Measuring tape			
Roughness	Against reference chart			
Wall strength	Schmidt hammer			
Aperture	Feeler gauge			
Filling	Visual			
Seepage	Timed observations			
Number of sets	Stereographic projection			
Block size	3-D fracture frequency			

A11.2 The completed table follows. These measurements cover a wide range of attributes — rock mass geometry, intact rock strength and

Characteristic	Measurement method	Core	B/H wall	Exposure
Orientation	Compass-clinometer	M	G	G
Spacing	Measuring tape	G	G	G
Persistence	Measuring tape	P	P	G/M
Roughness	Against reference chart	M	P	G
Wall strength	Schmidt hammer	M	P	G
Aperture	Feeler gauge	P	M	G
Filling	Visual	P	P	G
Seepage	Timed observations	P	P/M	G
Number of sets	Stereographic projection	M	G	G
Block size	3-D fracture frequency	P	P	G

hydrogeological properties. Also, some of the measurements are more easily performed during one type of site investigation than another. Although there is, therefore, some subjectivity in the G, M, P quality coding, the completed table should be of this general form.

Q11.3 **The results of a series of scanline surveys at a particular site are as follows:**

Scanline trend (°)	**000**	**355**	**085**	**153**	**216**	**271**
Scanline plunge (°)	**90**	**35**	**28**	**51**	**05**	**12**
Fracture frequency (m^{-1})	**5.54**	**7.93**	**6.02**	**7.00**	**6.99**	**7.65**

Analysis of the fractures intersected by the scanlines has shown that the rock mass contains four fracture sets, with orientations 145/08, 148/88, 021/76 and 087/69 (given as dip direction/dip angle). What is the best estimate of the frequency of each fracture set?

A11.3 For the situation when we know the orientation and fracture frequency of each of the four fracture sets, then the fracture frequency along a scanline in any particular direction, Λ_s, is given by (see A7.6)

$$\Lambda_s = \lambda_1 |\cos\theta_{s1}| + \lambda_2 |\cos\theta_{s2}| + \lambda_3 |\cos\theta_{s3}| + \lambda_4 |\cos\theta_{s4}|$$

where θ_{s1} is the angle between the normal to Set 1 and the direction in which we are interested, and the other angles are similarly defined.

If we write out this equation for each scanline, and arrange the results in matrix form, we obtain

$$\begin{bmatrix} \Lambda_1 \\ \Lambda_2 \\ \vdots \\ \Lambda_6 \end{bmatrix} = \begin{bmatrix} |\cos\theta_{11}| & |\cos\theta_{12}| & \cdots & |\cos\theta_{14}| \\ |\cos\theta_{21}| & |\cos\theta_{22}| & \cdots & |\cos\theta_{24}| \\ \vdots & \vdots & \vdots & \ddots \\ |\cos\theta_{61}| & |\cos\theta_{62}| & \cdots & |\cos\theta_{64}| \end{bmatrix} \begin{bmatrix} \lambda_1 \\ \lambda_2 \\ \vdots \\ \lambda_4 \end{bmatrix} \quad \text{or} \quad \boldsymbol{\Lambda} = \boldsymbol{\Omega} \cdot \boldsymbol{\lambda}$$

Hence, for the case when the vector $\boldsymbol{\Lambda}$ is known (i.e. the scanline results) and the vector $\boldsymbol{\lambda}$ is unknown (i.e. the fracture set frequencies), we need to solve this matrix equation for $\boldsymbol{\lambda}$. However, as the matrix $\boldsymbol{\Omega}$ has more rows than columns, it cannot be simply inverted, and so the best estimate for $\boldsymbol{\lambda}$ is given by the least-squares solution,

$$\boldsymbol{\lambda} = \left(\boldsymbol{\Omega}^{\mathrm{T}} \cdot \boldsymbol{\Omega}\right)^{-1} \cdot \left(\boldsymbol{\Omega}^{\mathrm{T}} \cdot \boldsymbol{\Lambda}\right).$$

In order to evaluate this equation, we firstly determine the angles between the individual scanlines and the normals to the fracture sets. These angles can either be computed using vector methods, or measured on the hemispherical projection. Using the former method leads to the following results for the angles:

	Set 1	Set 2	Set 3	Set 4
Scanline 1	8.0	88.0	76.0	69.0
Scanline 2	48.2	41.5	125.1	76.6
Scanline 3	66.2	112.6	105.2	131.0
Scanline 4	46.9	126.8	53.4	87.7
Scanline 5	87.6	111.7	17.3	51.9
Scanline 6	73.4	57.3	68.0	9.8

and from this we obtain the matrix of $|\cos\theta_{si}|$ values,

$$\Omega = \begin{bmatrix} 0.990 & 0.035 & 0.242 & 0.358 \\ 0.667 & 0.749 & 0.576 & 0.232 \\ 0.403 & 0.384 & 0.262 & 0.656 \\ 0.683 & 0.599 & 0.597 & 0.040 \\ 0.041 & 0.370 & 0.955 & 0.617 \\ 0.286 & 0.540 & 0.375 & 0.985 \end{bmatrix}.$$

As a result, the frequencies of the fracture sets are found to be

$$\lambda = \left(\Omega^{\mathrm{T}} \cdot \Omega\right)^{-1} \cdot \left(\Omega^{\mathrm{T}} \cdot \Lambda\right) =$$

$$\begin{bmatrix} 2.138 & 1.268 & 1.283 & 1.108 \\ 1.268 & 1.498 & 1.454 & 1.222 \\ 1.283 & 1.454 & 1.867 & 1.374 \\ 1.108 & 1.222 & 1.374 & 1.965 \end{bmatrix}^{-1} \times \begin{bmatrix} 20.457 \\ 19.360 \\ 21.200 \\ 19.899 \end{bmatrix} = \begin{bmatrix} 3.42 \\ 3.91 \\ 3.54 \\ 3.29 \end{bmatrix} \mathrm{m}^{-1}.$$

Knowing the fracture frequencies of the sets enables the calculation of the fracture frequencies along lines of any orientation in a rock mass, as required in the next question in which the fracture frequencies have been slightly changed.

***Q11.4* As part of a site investigation study, a rock mass was found to contain four fracture sets with dip/dip direction and frequencies as follows (see figure on next page):**

Set 1: 08/145, 3.48/m
Set 2: 88/148, 3.91/m
Set 3: 76/021, 3.58/m
Set 4: 69/087, 3.26/m

In order to establish in which directions through the rock mass an excavation will encounter the minimal and maximal numbers of fractures, the fracture frequency in different directions through the rock mass, λ_s, was calculated using the formula $\lambda_s = \sum_{i=1}^{n} |\lambda_i \cos\theta_i|$ (see Q7.6 and A7.6). The results are presented below on a hemispherical projection, with the contouring corresponding to the fracture frequency values in the different directions.

Explain from first principles why the directions of the minimal and maximal frequencies occur where they do.

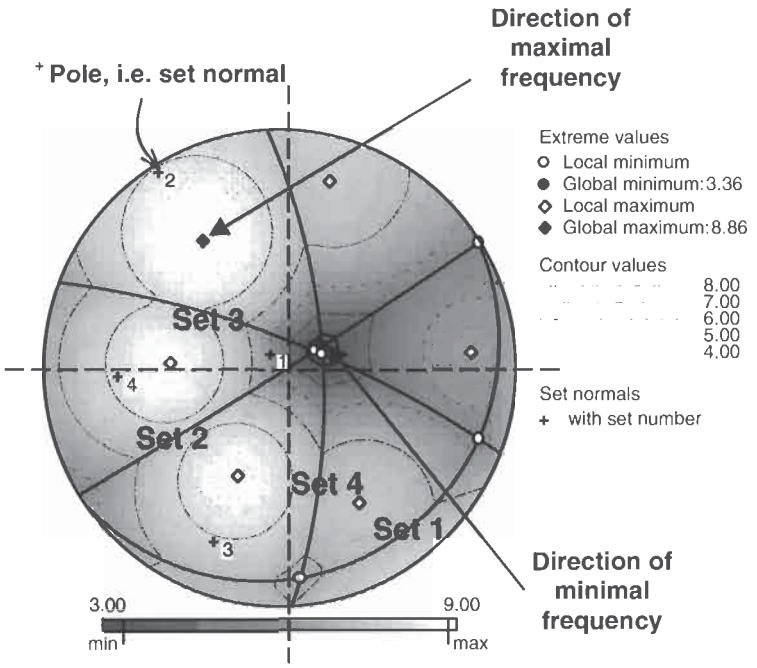

A11.4 *Minimal value.* In any given rock mass, the minimum fracture frequency lies along a direction that is formed by the intersection of two fracture sets. This is because no fractures from the relevant fracture sets will be intersected along such a direction. To identify the global frequency minimum we therefore need to determine the direction of the intersection of each pair of fractures, and then compute the fracture frequency in that direction. The directions of the various intersections, and the frequency computed along those directions, are as follows:

Sets 1 and 2	Sets 1 and 3	Sets 1 and 4	Sets 2 and 3	Sets 2 and 4	Sets 3 and 4
058/00	109/07	174/07	064/71	063/67	072/68
5.42 m^{-1}	5.68 m^{-1}	6.65 m^{-1}	3.44 m^{-1}	3.36 m^{-1}	3.38 m^{-1}

The global minimum is therefore in the direction of the intersection of Sets 2 and 4, and has a magnitude of 3.36 m^{-1}. Notice that the minima in the directions of the intersections of Sets 2 and 3, Sets 2 and 4, and Sets 3 and 4 are all similar in magnitude. This is because the directions of these intersections are all similar.

Maximal value. Although the directions of the various minima coincide with the directions of fracture set intersections, the directions of the various maxima are not so well defined and can only be found by rigorous computation. The maximal value occurs where the sum of the fracture contributions from all intersected sets is maximized, and an approximate value could be found by simply scanning all the fracture frequency values used to generate the contoured hemispherical projection to find the maximum value.

A more elegant method utilizes the vector-like nature of fracture frequency (i.e. it has both a magnitude and a direction): the maximal fracture frequency is found as the resultant of the individual set frequencies. However, because the maximal frequency for each fracture set occurs in two opposite directions (e.g. for a horizontal set the maximal frequency occurs in both a vertical upward and a vertical downward direction), the resultant formed from either of these directions must be considered.

Clearly, therefore, a number of candidates for the overall maximum will be found using this procedure. In fact, these will either be the various local maxima that can be seen in each zone of the projection bounded by great circles, or maxima that — whilst mathematically valid — do not physically exist. To identify which is which, the actual frequency in the direction of a mathematical maximum is computed and the two results compared; they are equal for maxima that physically exist.

In order to investigate the various maxima shown on the projection, we start by computing the Cartesian components of the normal to each fracture set. For a right-handed set of axes with x directed east, y directed north and z directed upwards, these components are given by $n_x = \sin(\alpha_n)\cos(\beta_n)$, $n_y = \cos(\alpha_n)\cos(\beta_n)$ and $n_z = -\sin(\beta_n)$, where α_n and β_n are the trend and plunge of the normal. For the fracture sets used here, these are as follows:

α	β	α_n	β_n	n_x	n_y	n_z
145	08	325	82	−0.080	0.114	−0.990
148	88	328	02	−0.530	0.848	−0.035
021	76	201	14	−0.348	−0.906	−0.242
087	69	267	21	−0.932	−0.049	−0.358

These values represent downward-directed normals, and to convert them to upwards-directed normals we simply multiply each component by −1. The components of each of the various resultants are then given as $r_x = \sum_i s_i n_{x_i}$, $r_y = \sum_i s_i n_{y_i}$ and $r_z = \sum_i s_i n_{z_i}$, where each s_i takes the value ±1 in order to cycle through all candidate resultants. Applying these to the data used here results in the table given below.

Candidate	s_1	s_2	s_3	s_4	$r_x = \sum_i s_i n_{x_i}$	$r_y = \sum_i s_i n_{y_i}$	$r_z = \sum_i s_i n_{z_i}$	Resultant
1	1	1	1	1	−6.633	0.308	−5.617	8.697
2	1	1	1	−1	−0.554	0.627	−3.280	3.385
3	1	1	−1	1	−4.143	6.794	−3.885	8.855
4	1	1	−1	−1	1.936	7.113	−1.548	7.532
5	1	−1	1	1	−2.491	−6.319	−5.344	8.643
6	1	−1	1	−1	3.587	−6.001	−3.007	7.611
7	1	−1	−1	1	−0.002	0.167	−3.612	3.616
8	1	−1	−1	−1	6.077	0.485	−1.275	6.228

The Cartesian components of each candidate are found by normalizing each resultant in the table above to a magnitude of unity. If we represent

these Cartesian components by (m_x, m_y, m_z), they are used in the usual formula of

$$\lambda_s = \sum_i \lambda_i |\cos(\theta_i)| = \sum_i \lambda_i |m_x n_{x_i} + m_y n_{y_i} + m_z n_{z_i}|$$

to compute the actual frequency in the direction they represent. This computation, together with the magnitude of the resultant shown above, is given below.

Candidate	m_x	m_y	m_z	$\lambda_1\lvert\cos(\theta_1)\rvert$	$\lambda_2\lvert\cos(\theta_2)\rvert$	$\lambda_3\lvert\cos(\theta_3)\rvert$	$\lambda_4\lvert\cos(\theta_4)\rvert$	λ_s, m^{-1}	Resultant
1	−0.763	0.035	−0.646	2.452	1.785	1.394	3.067	8.697	8.697
2	−0.164	0.185	−0.969	3.458	1.085	0.442	1.600	6.585	3.385
3	−0.468	0.767	−0.439	1.946	3.571	1.526	1.812	8.855	8.855
4	0.257	0.944	−0.206	1.012	2.625	3.204	0.691	7.532	7.532
5	−0.288	−0.731	−0.618	1.921	1.742	3.265	1.715	8.643	8.643
6	0.471	−0.788	−0.395	0.918	3.535	2.312	0.845	7.611	7.611
7	0.000	0.046	−0.999	3.461	0.290	0.716	1.161	5.628	3.616
8	0.976	0.078	−0.205	0.465	1.734	1.290	2.739	6.228	6.228

This shows that candidates 2 and 7 do not physically exist. Of the remaining candidates, their orientations are found from their Cartesian components to be 273/40, 329/26, 015/12, 202/38, 149/23, and 085/12. Of these, the global maximum is at 329/26 with a magnitude of 8.855 m^{-1}.

This answer illustrates an important point: **the directions corresponding to the minimal and maximal numbers of intersected fractures are not perpendicular**. The reason why this is important is that it raises questions about the validity of tensor representations of rock mass properties, in which the principal directions corresponding to the extreme values are orthogonal, as is the case for stress, strain and permeability. For example, we saw in Q8.3 and A8.3 that the directions of minimal and maximal rock mass deformability modulus may not be perpendicular.

***Q11.5* When cyclic deformability tests are conducted on rock masses, the typical force–displacement curve is as shown to the right (Schneider, 1967[3]; Goodman, 1989).**

Explain why, with cycles of repeated unloading and reloading, the curve manifests different unloading and reloading moduli, permanent deformations and hysteresis.

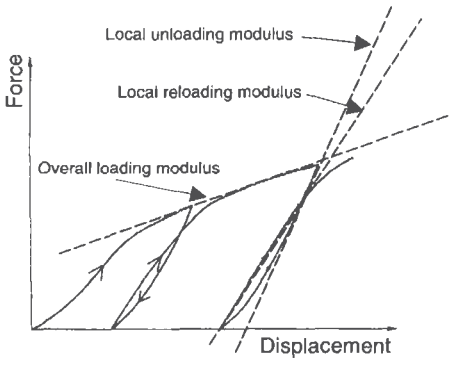

[3] Schneider B. (1967) Moyens Nouveaux de Reconnaissance des Massifs Rocheux. *Supp. to Annales de l'Inst. Tech. de Batiment et des Travaux Publics*, **20**, 235–236, 1055–1093 (as illustrated in Goodman R. E. (1989) *Introduction to Rock Mechanics*, 2nd edn., John Wiley and Sons, New York, 562pp).

A11.5 The mechanical behaviour of a rock mass is dominated by the fractures, which significantly reduce the modulus from the intact rock value. The deformation modulus of a rock mass is often only about one tenth that of the intact rock modulus. Thus, we would expect that the idiosyncrasies of the force–displacement curve above are caused by the fractures. Indeed, when fractures are compressed, they have a non-linear behaviour as the asperities are deformed and crushed. However, when the fractures are subsequently unloaded, the behaviour will be more linearly elastic and stiffer, because the asperities have been crushed. This is also the reason for the permanent deformation and the hysteresis that occurs on initial loading and unloading. After one or two cycles of such loading and unloading, the fracture surfaces in the rock mass have been sufficiently disturbed to make the rock mass modulus higher and it responds in a more reproducible manner. The site investigation question is which modulus the design calculations require — and this will depend on whether the rock mass will be repeatedly loaded during engineering operations.

Q11.6 **The tensile strength of an architectural granite was measured to ensure that the granite would be strong enough to form the structural elements of a pedestrian bridge in a shopping mall. Ten specimens were tested in each of four test configurations (illustrated in A6.9), and the values obtained were as follows.**

Type of test	Mean value (MPa)	Standard deviation (MPa)
Direct tension test	8.4	3.2
Point load test	9.6	3.8
Beam test	10.4	4.5
Ring test	12.9	6.7

Are these results consistent with what you know about tensile strength variation and which value would you use for the structural calculations?

A11.6 We expect tensile strength variation (see A6.9) both within and between tests. The tensile strength increases with (a) a lower test volume subjected to the high stress, and (b) a higher tensile stress gradient. We note that the different tensile strength test configurations have the following characteristics.

Direct tension test. The whole test volume is subject to the same high tensile stress and there is no tensile stress gradient. This indicates a low measured strength.

Point load test. The region of the specimen between the loading platens is subjected to a high tensile stress, and there is no significant tensile stress gradient.

Beam test. It is only the region at the opposite face of the beam from the loading point that is subjected to the high tensile stress, where there is a linear tensile stress gradient.

Ring test. Only the regions on the inner surface in line with the loading are subjected to the high tensile stress, where there is a steep tensile stress gradient. This results in a high measured strength.

Thus, the mean values and standard deviations of the test results are entirely consistent with our understanding of tensile strength variation. For the structural calculations, we should use the value obtained in a similar configuration to the design configuration, i.e. the beam test. We should also obtain an estimate of any scale effect in moving up to the size of the bridge elements, and apply a safety factor.

***Q11.7* The following table shows data obtained from a single-stage triaxial compression test on a cylindrical rock sample, conducted with closed-loop servo-control, at a confining stress of 10.0 MPa, and at zero pore pressure.**

Total axial load (kN)	Sample height (mm)	Sample diameter (mm)
0.00	100.84	50.20
19.89	100.80	50.20
39.60	100.77	50.20
63.40	100.74	50.20
88.67	100.71	50.21
116.18	100.68	50.21
144.68	100.65	50.22
162.38	100.63	50.22
185.23	100.58	50.24
190.62	100.56	50.25
191.99	100.54	50.25
180.22	100.52	50.26
137.56	100.49	50.26
115.79	100.46	50.27
101.93	100.43	50.28
97.97	100.40	50.28
96.98	100.37	50.28

Estimate values for the following:
(i) yield strength σ_y;
(ii) peak strength σ_{max};
(iii) residual strength σ_r;
(iv) tangent Young's modulus E_{tan} at 50% peak axial stress; and
(v) tangent Poisson's ratio ν_{tan} at 50% peak axial stress.

A11.7 From the test data recorded, we compute the axial stress, axial strain and diametral strain in order to plot the axial stress–axial strain and diametral strain–axial strain curves and to visually estimate the various strength parameters. The stress and strain values are given in the table below. Note that the axial strain values are positive (because the convention of contraction positive is being used), but the diametral strain values are negative (because the specimen expands circumferentially during the compression test).

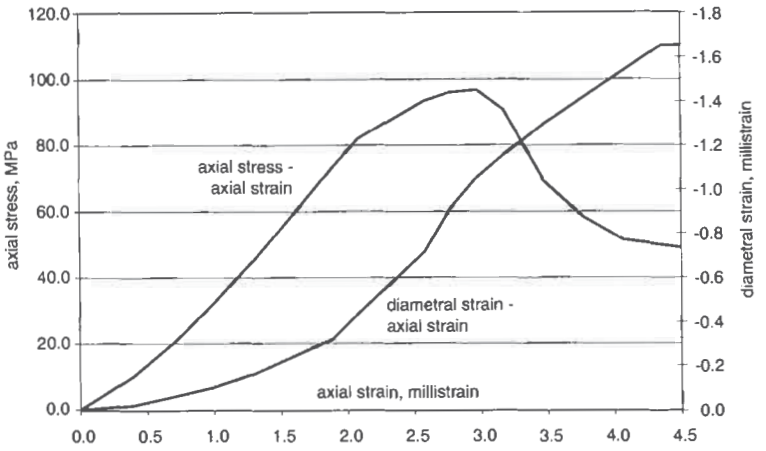

The curves associated with these results are shown above. The strength parameters are read from these curves, and have the following values:

(i) yield strength $\sigma_y \approx 83$ MPa (this is where the axial stress–axial strain curve becomes visibly non-linear);

(ii) peak strength $\sigma_{max} \approx 97$ MPa (this is the maximum axial stress the specimen sustained);

(iii) residual strength $\sigma_r \approx 49$ MPa (this is the final stress value given, which may have reduced further had the test been continued);

(iv) tangent Young's modulus E_{tan} at 50% peak axial stress is computed from the axial stress and axial strain values immediately above and below 50% of the peak axial stress. The value is given by

$$\frac{58.70 - 44.80}{1.171 - 0.893} = \frac{13.9}{0.278} = 50.00 \text{ GPa}.$$

In practice, we would compute this value from several ranges of values to estimate any variation.

Axial stress	Axial strain	Diametral strain
0.00	0.000	0.000
10.05	0.397	−0.020
20.01	0.694	−0.060
32.03	0.992	−0.100
44.79	1.289	−0.159
58.67	1.587	−0.239
73.05	1.884	−0.319
81.97	2.083	−0.438
93.45	2.578	−0.717
96.13	2.777	−0.916
96.80	2.975	−1.056
90.85	3.173	−1.155
69.32	3.471	−1.295
58.34	3.768	−1.414
51.34	4.066	−1.534
49.34	4.363	−1.653
48.84	4.661	−1.653

(v) tangent Poisson's ratio ν_{tan} at 50% peak axial stress is similarly computed from the diametral and axial strain values immediately above and below 50% of the peak axial stress. It is given by

$$\frac{0.159 - 0.100}{1.171 - 0.893} = \frac{0.059}{0.278} = 0.21.$$

***Q11.8* Explain why the introduction of servo-controlled testing machines in the early 1970s revolutionized rock mechanics laboratory testing, and why we are now able to test rocks under virtually any loading conditions.**

A11.8 The principle of a servo-controlled testing machine is that a feedback signal representing some experimental value is continuously

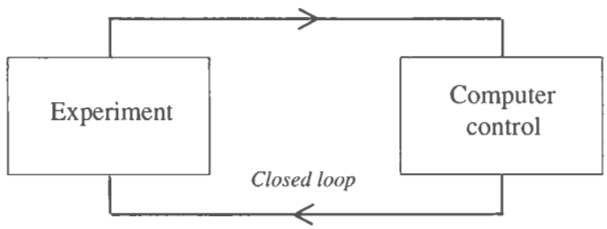

compared with a program signal representing the desired value: any discrepancy is corrected with only a 5 millisecond response time. This is known as a closed-loop control system.

Two complete stress–strain curves for rock are shown in the plot to the right. The pre-peak portion is the region OA. The two types of curve are categorized in terms of the characteristic of the post-peak region: either the curve monotonically increases in axial strain (the thick curve) or it does not (the thinner curve). The former, is termed a Class I curve; the latter is termed a Class II curve (Fairhurst and Hudson, 1999[4]).

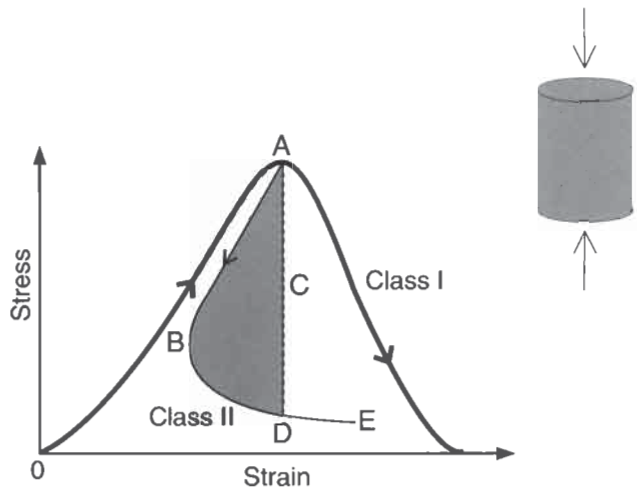

It is important to understand these two types of curve in order to optimize the control of rock failure. Cylindrical specimens that exhibit Class I behaviour tend to be somewhat ductile in nature when loaded axially, whereas specimens that exhibit Class II behaviour respond in a brittle fashion to axial loading. A test conducted in axial strain control is generally sufficient to obtain the complete stress–strain curve of specimens exhibiting Class I behaviour, but alternative control techniques, such as using circumferential strain as the independent (or control) variable, are necessary when testing specimens that exhibit Class II behaviour because the stress–strain curve does not then monotonically increase in axial strain. Note that the shaded area ABDCA is the surplus energy which would be supplied by a rigid machine (one with infinite

[4] Fairhurst C. E. and Hudson J. A. (1999) Draft ISRM suggested method for the complete stress–strain curve for intact rock in uniaxial compression. *Int. J. Rock Mech. Min. Sci.*, **36**, 3, 279–289.

stiffness indicated by the line AD) or a servo-controlled machine with axial strain control — both leading to uncontrolled failure — and so energy has to be withdrawn from the specimen to sustain continued controlled failure. It is an awesome experience to stand next to a granite specimen being tested under such controlled conditions and watch it quietly change from solid rock to fragmented grains and dust particles.

In a uniaxial compression test, one could, for example, control the stress rate, the strain rate, the energy input rate, the pore pressure, or the acoustic emission output rate. Servo-control can be used in any testing configuration and this type of testing machine is limited only by one's imagination. That is why such machines have revolutionized rock testing and enable virtually any test to be servo-controlled. Also, more realistic loading conditions can be applied, so that the rock can be tested in the same way that it is loaded in the engineering scheme. We anticipate that the next phase of development will be the use of servo-control in field tests.

***Q11.9* (a) The results in the table below represent shear displacement and shear stress recorded during a direct shear test on a fracture in slate. The shear displacement range was from 0 to 15 mm as shown in the table below. The normal stress during the test was 0.34 MPa.**

Shear displacement (mm)	**0.0**	**0.5**	**1.0**	**1.5**	**2.0**	**2.5**	**3.0**	**3.5**
Shear stress (kPa)	**0**	**281**	**344**	**344**	**328**	**281**	**281**	**297**
Shear displacement (mm)	**4.0**	**4.5**	**5.0**	**5.5**	**6.0**	**6.5**	**7.0**	**7.5**
Shear stress (kPa)	**281**	**281**	**266**	**266**	**266**	**281**	**281**	**281**
Shear displacement (mm)	**8.0**	**8.5**	**9.0**	**9.5**	**10.0**	**10.5**	**11.0**	**11.5**
Shear stress (kPa)	**297**	**297**	**297**	**313**	**313**	**313**	**313**	**313**
Shear displacement (mm)	**12.0**	**12.5**	**13.0**	**13.5**	**14.0**	**14.5**	**15.0**	
Shear stress (kPa)	**313**	**313**	**313**	**313**	**313**	**313**	**313**	

Use these results to determine the residual shear strength of the fracture.

(b) A series of direct shear tests was undertaken at different normal stress values on samples from the fracture, and the peak shear stress encountered during each test was recorded, as shown in the table below.

Normal stress (kPa)	**336**	**648**	**961**	**1273**	**1586**
Peak shear stress (kPa)	**344**	**516**	**719**	**953**	**1156**

Use these results to determine the basic friction angle, ϕ, and the asperity angle, i, for the fracture. Also comment on the validity of the bi-linear approximation for the failure locus.

A11.9 This question has been included to illustrate typical laboratory testing results and their interpretation. Such laboratory testing is invariably conducted if specific properties are required for an analytical or numerical model. It is therefore essential that we know how to extract

such values from test results — which is sometimes straightforward, and sometimes open to interpretation.

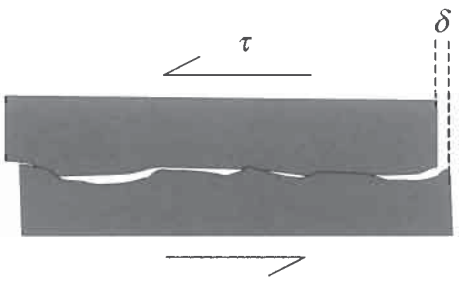

Schematic cross-section of the direct shear test

(a) Plotting the displacement and stress results for the shear test, illustrated above, generates the diagram shown below. There is a well-defined peak strength, followed by a poorly defined residual strength. By poorly defined, we mean that a residual strength is encountered at a displacement of about 6 mm, but should the residual strength be this or the one reached at a larger maximum displacement? Although, by definition, we regard the residual strength as that reached at large displacements, this may not be appropriate if the fracture has failed at some intermediate lower strength — before reaching the higher strength attained at a larger displacement.

By analogy with the complete stress–strain curve in compression, the *in situ* stability of the fracture depends on the stiffness of the loading system (i.e. the engineering structure for a field project), and the appropriate value for the residual strength can only be chosen given the engineering circumstances. Thus, it may be that the appropriate residual shear strength is either about 260 kPa or about 310 kPa. If a shear displacement of more than 8 mm is sufficient to cause catastrophic collapse of a structure, it is of no value to know what the strength would be at subsequent, higher, shear displacement values.

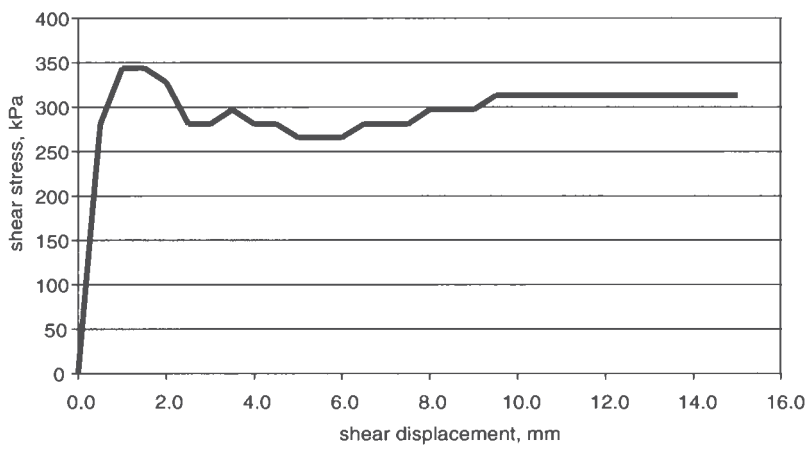

(b) Plotting the normal stress and peak shear stress values provides a failure locus, and the values lie close to a straight line, as shown below. The basic friction angle is given by the slope of this straight line, 33.4°.

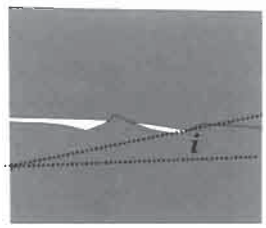

The asperity angle *i*

The bi-linear approximation to the failure locus requires that the initial portion of the locus emanates from the origin. However, there is no way of determining where this initial portion intersects the measured failure locus — we have assumed it to be where the locus intersects the normal stress used in the first test. The dashed extension of the measured failure locus is fictitious, and is sometimes used to determine an 'apparent cohesion'. To compute the asperity angle, i, we take the gradient of the initial segment of the locus, $\phi + i$, which has a value of 44°, and subtract from it the basic friction angle ϕ, to give an asperity angle of $44° - 33.4° = 10.6°$.

All five of the test results lie close to a straight line, and hence indicate that any bi-linear behaviour would occur at a normal stress value lower than the smallest one used here. We have assumed that the initial part of the bi-linear approximation extends between the origin and the first test result, but there is no means of establishing this on the basis of the results given.

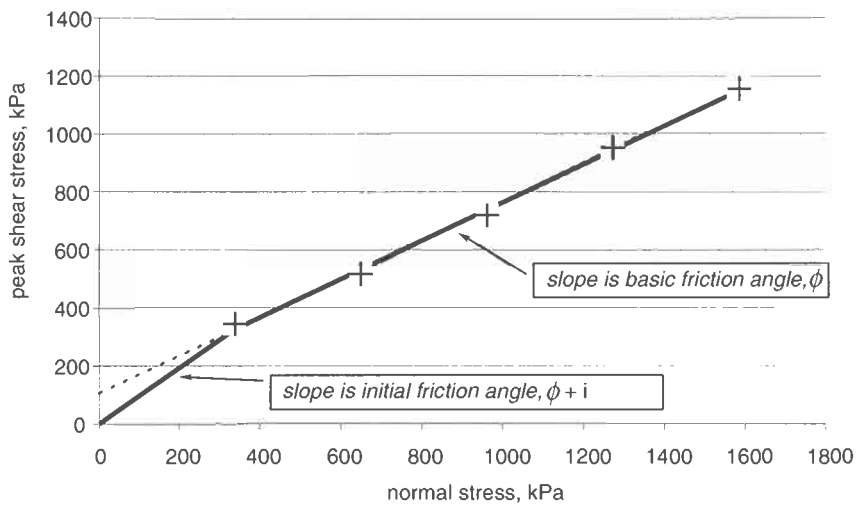

Q11.10 **The diagram below shows example results from using a numerical modelling code for predicting the elastic displacements (indicated by the arrows) of a 2-D assemblage of distinct rock blocks through which a tunnel has been excavated. The plot shows the displacement vectors.**

(a) Write down a list of rock properties that you think would be required as input to such a modelling exercise.

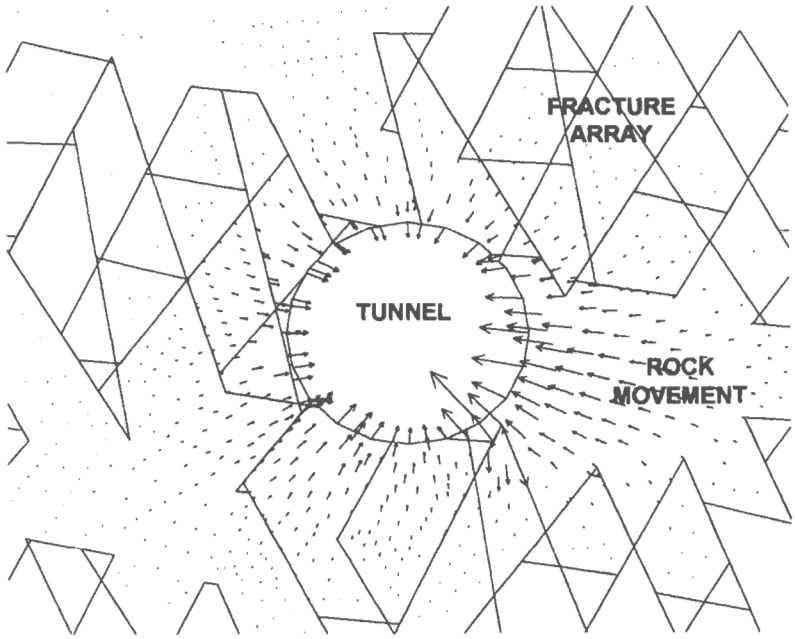

(b) Indicate which of these are likely to be practicably measureable.

A11.10 (a) There are many possible answers to this question, but the rock parameters actually used by the UDEC code which generated the results are:

- the magnitudes and directions of the *in situ* principal stresses;
- Young's modulus and Poisson's ratio of the intact rock;
- the number of fracture sets and;
- for each fracture set, the orientation, frequency, persistence, cohesion, angle of friction, normal stiffness, shear stiffness, and dilation angle.

(b) The *in situ* stress state and intact rock parameters can usually be established fairly well, assuming homogeneity across the region of interest. The number of fracture sets is sometimes clear, but sometimes not in complex circumstances. Given that fracture sets have in fact been established, the orientation and frequency are relatively easy to specify, but the persistence is impossible to measure completely and hence to specify. The cohesion and angle of friction are also relatively easy to measure or estimate, but establishing values for the normal stiffness, shear stiffness and dilation angle that represent the *in situ* fractures is much more difficult.

Thus we see that a disadvantage of such numerical modelling is that a large proportion of the required input parameters may not be obtainable. However, the advantage of the numerical modelling approach is that the sensitivity of the instability mechanisms to the input parameters can be studied in detail. Thus, it is better to use numerical modelling for a parametric study of the overall rock mass behaviour, rather than trying to establish specific values at specific points in the rock mass.

11.3 Additional points

We emphasize that it is not possible to specify the components of a site investigation and the associated testing programme that will be universally appropriate for all rock engineering projects. This is because different projects have different objectives (e.g. the objective of mining engineering is to obtain the rock, whereas the objective of civil engineering is to utilize the space created). Thus, it is necessary to understand the complexities of the rock mass geometry and mechanical properties in order to make sensible decisions on the optimal site investigation given a specific engineering objective.

Sometimes, even the most basic parameters cannot be measured directly. For example, assume that you have been contracted to measure the rock stresses during a site investigation. The client, who takes an interest in rock mechanics, visits your measurement site. He is watching you using the flatjack technique — measuring the normal rock stress components. You have installed two pins in a rock wall, measured the distance between them, cut a slot in the rock wall between the pins, cemented a 'flatjack' into the slot, and hydraulically inflated the jack until the original distance between the pins is re-established, giving the normal stress component perpendicular to the flatjack. The client asks you how many measurements you are going to make. You explain that there will be six such normal rock stress measurements at each test location, using six flatjacks at six orientations, so that the six normal stresses can be used to establish the three normal stresses and three shear stresses of the rock stress matrix. Suddenly, the client has an inspiration, "Surely, it would be better and more elegant to measure the three normal stresses and the three shear stresses directly, rather than measuring six normal stresses?" The client's inspiration is a good idea but, unfortunately, no one has yet found a way to measure a shear stress directly.

For standardization, it is necessary to have guidance on how to establish specific rock parameters. The International Society for Rock Mechanics (ISRM) and the American Society for Testing Materials (ASTM) publish recommended procedures for establishing a wide range of parameters. We gave lists of these in Chapter 11 of ERM 1. Starting in 1998, a second series of ISRM Suggested Methods has been under development; these can be found in the issues of the International Journal of Rock Mechanics and Mining Sciences from 1999 onwards (e.g. see Fairhurst and Hudson, 1999).